Title

The Role of Amplicon Length and Total DNA Length in Synthetic DNA Tracer Degradation and Adsorption During Transport Through Sand

Journal

Water Resources Research, 62(6)

ISSN

0043-1397

Authors

Liu, Geng

Wang, Chaozi

Dahlke, Helen E

et al.

Publication Date

2026-06-01

DOI

10.1029/2025wr042716

Water Resources Research

RESEARCH ARTICLE
10.1029/2025WR042716

The Role of Amplicon Length and Total DNA Length in Synthetic DNA Tracer Degradation and Adsorption During Transport Through Sand

Geng Liu[1], Chaozi Wang[1,2], Helen E. Dahlke[3], M. Todd Walter[4], En Xie[1], Xiao Zhao[1], Guanhua Huang[1,5], Quanzhong Huang[1,5], Xin He[1], Xinfeng Wang[1], Jiarong Liu[1], Zengjie Hu[1], Yuhan Zhang[1], Haoqi Guo[1], Zhen Wang[1], Pu Wang[1], Weishu Wang[1], Chenglong Zhang[1,2], and Zailin Huo[1,2]

[1]State Key Laboratory of Efficient Utilization of Agricultural Water Resources, China Agricultural University, Beijing, China, [2]Center for Agricultural Water Research in China, China Agricultural University, Beijing, China, [3]Department of Land, Air, and Water Resources, University of California, Davis, Davis, CA, USA, [4]Department of Biological and Environmental Engineering, Cornell University, Ithaca, NY, USA, [5]Bayannur Research Institute China Agricultural University, Bayannur, China

Abstract Synthetic DNA tracers are increasingly used in subsurface hydrological studies because their large sequence diversity enables the design of numerous uniquely identifiable tracers. However, previous studies have not isolated how amplicon length, flanking region length, and total DNA length independently control tracer degradation and adsorption during subsurface transport. In this study, eight double-stranded DNA (dsDNA) tracers with systematically varied amplicon and total sequence lengths were designed to disentangle the effects of these dsDNA tracer design parameters. Batch degradation experiments were conducted in two types of waters to determine degradation rates, and column transport experiments in two types of sand media were performed to evaluate adsorption behavior. Adsorption and degradation losses during transport were separated using calibrated kinetic sorption models. Results show that degradation rates of dsDNA tracers are primarily controlled by amplicon length rather flanking region length. Tracers with identical amplicon lengths but different flanking region lengths exhibited similar degradation rates, whereas tracers with longer amplicons degraded significantly faster. In contrast, adsorption behavior was governed by the total DNA length, with adsorption increasing linearly with sequence length in both Ottawa sand ($y = 0.0013x + 0.370$, $R^2 = 0.934$) and finer quartz sand ($y = 0.0006x + 0.724$, $R^2 = 0.999$), while detachment rate constants decreased linearly with increasing length. These findings demonstrate that degradation and adsorption are controlled by the dsDNA tracer design parameters and provide a mechanistic basis for designing tracers with predictable transport behavior in subsurface hydrological systems.

Key Points:

- Degradation of double-stranded DNA (dsDNA) tracers is controlled by amplicon length
- Adsorption (%) increases linearly with total DNA length
- Desorption rate (k_{d1}) decreases linearly with an increase in total dsDNA length

Supporting Information:

Supporting Information may be found in the online version of this article.

Correspondence to:

C. Wang,
chaoziwang@cau.edu.cn

Citation:

Liu, G., Wang, C., Dahlke, H. E., Walter, M. T., Xie, E., Zhao, X., et al. (2026). The role of amplicon length and total DNA length in synthetic DNA tracer degradation and adsorption during transport through sand. *Water Resources Research*, *62*, e2025WR042716. https://doi.org/10.1029/2025WR042716

Received 17 NOV 2025
Accepted 13 JUN 2026

Author Contributions:

Conceptualization: Geng Liu, Chaozi Wang
Formal analysis: Geng Liu
Funding acquisition: Chaozi Wang, Zailin Huo
Investigation: Geng Liu, Chaozi Wang, Jiarong Liu, Zengjie Hu, Yuhan Zhang, Haoqi Guo, Zhen Wang, Pu Wang
Methodology: Geng Liu
Project administration: Chaozi Wang, Zailin Huo
Resources: Chaozi Wang, En Xie, Xiao Zhao, Guanhua Huang, Quanzhong Huang, Xin He, Xinfeng Wang
Supervision: Chaozi Wang, Helen E. Dahlke, M. Todd Walter, Zailin Huo
Validation: Geng Liu
Visualization: Geng Liu

1. Introduction

1.1. Synthetic DNA Tracers in Subsurface Hydrology

The use of synthetic DNA molecules as hydrological tracers has increased rapidly in recent years because they provide an essentially unlimited number of uniquely identifiable tracers (Foppen, 2023; Liao et al., 2018; Zhang & Huang, 2022). Synthetic DNA tracers typically consist of short single- or double-stranded DNA sequences, usually shorter than 400 nucleotides (nt) or base pairs (bp), which cannot replicate in natural environments (Pang et al., 2017; Wang, Liu, et al., 2022). Because each DNA sequence can act as a unique identifier, synthetic DNA tracers allow simultaneous tracking of multiple flow pathways within complex hydrological systems. For example, an 80 bp DNA sequence theoretically provides 4^{80} possible combinations, enabling the design of a very large number of distinguishable tracers.

This exceptional coding capacity makes DNA tracers particularly attractive for investigating subsurface transport processes, including groundwater flow, preferential flow pathways, and contaminant transport (Dahlke et al., 2015; Li et al., 2025).

1.2. Applications and Limitations of Single-Stranded DNA Tracers

Single-stranded DNA (ssDNA) tracers have been widely applied in subsurface hydrological studies to track flow pathways, especially under conditions where degradation is negligible. Early investigations demonstrated their

Writing – original draft: Geng Liu, Chaozi Wang
Writing – review & editing: Chaozi Wang, Helen E. Dahlke, M. Todd Walter, En Xie, Xiao Zhao, Guanhua Huang, Quanzhong Huang, Xin He, Xinfeng Wang, Jiarong Liu, Zengjie Hu, Yuhan Zhang, Haoqi Guo, Zhen Wang, Pu Wang, Weishu Wang, Chenglong Zhang, Zailin Huo

ability to identify multi-source groundwater contamination in sandy aquifers and fractured rock systems (Sabir et al., 1999, 2000). Later, Ptak et al. (2004) reported the first quantitative breakthrough curves of synthetic DNA tracers obtained from both undisturbed aquifer cores and in situ groundwater systems.

Subsequent studies expanded the application of ssDNA tracers to a wide range of environments, including fractured rock and karst aquifers, glacier hydrological systems, and soil-textured porous media (Aquilanti et al., 2013, 2016; Dahlke et al., 2015; Wang, Liu, et al., 2022). In packed soil experiments using crushed basaltic tephra, Wang, Liu, et al. (2022) reported minimal DNA degradation, which they attributed to the relatively sterile nature of the porous medium.

However, in natural soils and waters, DNA degradation is commonly driven by enzymatic breakdown mediated by bacteria and other microorganisms (Romanowski et al., 1993). DNA molecules may also adsorb strongly to mineral surfaces, particularly clay particles, through ligand exchange and van der Waals interactions, including hydrogen bonding (Liu et al., 2023). These degradation and adsorption processes can significantly influence tracer persistence and transport behavior.

To improve tracer stability and detection reliability, recent studies have explored alternative DNA tracer designs. For instance, Guo et al. (2025) developed multiple 80 bp DNA sequences that avoided hairpin and repetitive structures, enabling highly specific and simultaneous detection of multiple tracers in porous media flow systems.

1.3. Double-Stranded DNA Tracers and Remaining Knowledge Gaps

To further improve tracer stability, Pang et al. (2017, 2020) proposed double-stranded DNA (dsDNA) tracers consisting of an amplicon region flanked by protective DNA regions. In this design, the amplicon is uniquely sequenced and quantified using quantitative polymerase chain reaction (qPCR), enabling the differentiation of multiple tracers. The flanking regions are not amplified during qPCR but serve as protective buffers that shield the amplicon from degradation.

This design is partly motivated by observations that nucleotides at the ends of DNA strands may degrade at rates different from those located internally (Suzuki et al., 1994). Accordingly, protective flanking regions are introduced to reduce the likelihood that degradation processes affect the amplicon region used for detection (Pang et al., 2017, 2020).

Several dsDNA tracer designs have been proposed following this concept. For example, Seq-tracers developed by Pang et al. (2017) consisted of a unique 198 bp amplicon flanked by two identical 52 bp regions. Later, Pang et al. (2020) developed K-tracers with a 200 bp amplicon and longer 76 bp flanking regions. Batch experiments demonstrated that tracers with longer flanking regions degraded more slowly in stream water, groundwater, and wastewater effluents (Pang et al., 2022). However, the adsorption behavior of the tracers with longer flanking regions in sand media (e.g., the coastal aquifer media, alluvial aquifer media and the stream sediments) did not differ significantly from that of tracers with shorter flanking regions.

Other studies have investigated degradation patterns of dsDNA sequences, although without explicitly focusing on tracer amplicon-flanking design. For example, Mikutis et al. (2019) measured the degradation of a 113 bp dsDNA sequence and several shorter fragments derived from the same sequence. Their results suggested that degradation rates decreased with the length of qPCR quantified DNA fragment. When interpreted in the framework of amplicon-flanking designs, however, it remains unclear whether the observed differences were caused by the shorter amplicon or by the relatively longer flanking regions protecting the quantified fragment.

Adsorption processes introduce an additional layer of complexity. Zhang et al. (2021) investigated the transport of dsDNA tracers with total lengths ranging from 90 to 200 bp in sand columns. Their experiments indicated that longer DNA sequences exhibited stronger adsorption, which was attributed to multi-segment attachment of longer strands to sand surfaces. However, the quantitative relationship between DNA length and adsorption behavior has not been directly quantified with systematically varied DNA length. Moreover, it is unknown whether the relative proportions of amplicon length and flanking region length influence this relationship when the total DNA length is fixed.

Because previous studies have not independently controlled amplicon length, flanking region length, and total DNA length, it remains unclear how these three dsDNA tracer design parameters, govern degradation and adsorption processes individually. This raises three key questions: (a) whether degradation resistance is better

achieved by shortening the amplicon or extending the flanking regions; (b) how adsorption scales quantitatively with total DNA length; and (c) whether the relative proportion of amplicon and flanking regions influences adsorption behavior when total length is held constant.

1.4. Study Objectives and Approach

This study is designed specifically to disentangle previously confounded effects of amplicon length, flanking region length, and total DNA length by independently varying these three dsDNA tracer design parameters. This experimental separation enables direct attribution of degradation and adsorption processes to distinct components of tracer design. Building on this framework, this study addresses these questions through systematic tracer design and controlled laboratory experiments.

To investigate degradation mechanisms, two sets of dsDNA tracers were designed. The first set consisted of tracers with identical amplicon lengths but different flanking region lengths (A80F1, A80F10, and A80F20), allowing evaluation of whether longer flanking regions provide stronger protection against degradation. The second set consisted of tracers with identical total lengths but different amplicon lengths (A80F10 and A98F1), enabling assessment of whether shorter amplicons are inherently more resistant to degradation.

To investigate adsorption behavior, tracers with different total lengths (A80F1, A80F10, and A80F20) were used to examine potential quantitative relationships between DNA length and adsorption. In addition, tracers with identical total lengths but different amplicon-to-flanking ratios (A80F10 and A98F1) were used to determine whether the relative proportion of the amplicon length and flanking region length influences adsorption characteristics.

All tracer sequences were designed to avoid hairpin structures and repetitive motifs following the recommendations of Guo et al. (2025) to ensure high specificity and reliable qPCR detection.

The tracers were subjected to batch degradation experiments in two types of water and column transport experiments using two types of sand media. One-site and two-site kinetic sorption models were calibrated and validated using the experimental data to quantify adsorption and degradation processes independently during transport.

Through this combined experimental and modeling framework, this study aims to clarify the individual role of amplicon length, flanking region length, and total DNA length at controlling the independent degradation and adsorption behavior of dsDNA tracers, and to provide practical guidance for the design of DNA tracers for hydrological applications.

2. Materials and Methods

2.1. DsDNA Tracer Design

Eight dsDNA tracers with total lengths ranging from 82 to 120 base pairs (bp) were designed and synthesized for this study (Table 1). Each tracer comprised an amplicon region flanked by protective sequences on both ends, following the amplicon–flanking design proposed by Pang et al. (2017, 2020). The amplicon served as the target for qPCR, while the flanking regions provided protection against degradation. The minimum amplicon length (~80 bp) was determined by the sum of forward primer (18–25 bp), TaqMan probe (25–32 bp), reverse primer (18–25 bp), and junction region between 3′ end of forward primer and 5′ end of TaqMan probe (≥3 bp) (Figure 1b). The maximum total sequence length (~120 bp) was constrained by chemical synthesis efficiency (Masaki et al., 2022). All sequences were designed to avoid hairpin structures and repetitive structures to ensure high specificity and reliable qPCR detection (Guo et al., 2025).

To investigate the influence of flanking region length on degradation, three tracers with identical amplicon lengths (80 bp) but different flanking region lengths (1, 10, and 20 bp on each end) were designed: A80F1, A80F10, and A80F20, resulting in total lengths of 82, 100, and 120 bp (Figure 1a), respectively. To evaluate whether shortening the amplicon could enhance degradation resistance under fixed total length, tracer A98F1 was designed with a 98 bp amplicon and 1 bp flanking regions on each end (total length 100 bp, Figure 1a), enabling direct comparison with A80F10 (80 bp amplicon, 10 bp flanking regions). Together, these designs addressed the three research questions: (a) whether longer flanking regions or shorter amplicons better protect tracers from

Table 1
The Sequence, Primers and Probes of the Four Pairs of Synthetic dsDNA Tracers, Their Three dsDNA Tracer Design Parameters (Amplicon Length, Flanking Region Length and Total DNA Length), and qPCR Characteristics

Name	Sequence (5–3′) (bolded and underlined: Primers; bolded and italic: TaqMan probe)	Amplicon length [bp]	Flanking region length [bp]	Total length [bp]	qPCR efficiency [%]	R^2
A80F1_1	C**GACAAACGGCACGCTCTTG**AG TCA***ACGCTAGAGACAGCGGTCGGCAAA CCCAACG***ACG**AGTAATTGGTCAGTGG TTGCCA**C	80	1	82	93.2	1
A80F1_2	C**CCCGCCGTTATAGGCAAATAG**TAGT C***AGCTCGCGCTTCTGTCACAACGCTCCC ACA***GT**CACAATACAACGTGTGCAGGTA**C	80	1	82	96.2	0.999
A80F10_1	ATCAGCTAAC**GAGACGCGGAAACAT CCAT**GTCA***ACCACCACTCGCGTGCCCTCTT GCGGGTAA***CCTAC**TCCTAGTTGTCTGGTT AGTTGT**CCTAATGTGC	80	10	100	95.1	0.999
A80F10_2	ATCAGCTAAC**TGTTCTCCAGTCCCAAGT CGTT**AATA***CCTACGTCGTGATGCGTCCGG CACGTAGC***GTTCACGATCACTACAACT **AGCATA**CCTAATGTGC	80	10	100	90.7	0.999
A98F1_1	C**CGTAAACTTCCCGGTGTCATG**A***TCACA ACGTGGTCAGCTAAGCGCGCAGCCT***TATC AGTAGGCGAAGTATTGAAGCGA**ACTATT TCCGCATGGTTCTT**C	98	1	100	94.9	1
A98F1_2	C**CTCCCGTCCCGTTAGGTATC**GAAAAA ***CGTCAGCTCCGTCCTAGCGCCCATGGTTT CC***ATTTGGTCGTTGTAAAATCAG**CGTATT TGGGAGTGTGCGAG**C	98	1	100	95.1	0.999
A80F20_1	AAAGGCGAACATCAGCTAAC**GAATCTGAC GACGGTGCTAT***TCCATGGGTTGTGCCTGAA CCCAACCCGTCCT*CTATCT**AAGGACATGAT TTACAGCCTGG**CCTAATGTGCCACGACGCGT	80	20	120	93.5	0.999
A80F20_2	AAAGGCGAACATCAGCTAAC**CCGCTCAG TAGAAATTCGTTGA**CGTT***ACGCAGCCTGC GTTCGGCAGATGAACCGAA***ATT**AACTACA ACGCTTAGGCCACA**CCTAATGTGCCACG ACGCGT	80	20	120	95.6	0.999

degradation; (b) the quantitative relationship between total DNA length and adsorption behavior; and (c) the effect of amplicon-to-flanking ratios on adsorption at fixed total length.

To account for potential sequence-specific effects, two sequence variants were generated for each tracer type (e.g., A80F1_1 and A80F1_2), each with a unique randomly generated amplicon while maintaining identical flanking regions. Primer and probe binding sites for qPCR were included in each tracer, and the uniqueness of primers was confirmed via Primer-BLAST to avoid amplification of known genomic sequences (NCBI, 2023).

Complementary single-stranded DNA oligos were synthesized (Sangon Biotech, Shanghai) and annealed in pH 8.0 buffer to form dsDNA tracers (Jiang et al., 2015). The resulting dsDNA solutions were stored at −20°C until use, and their concentrations were determined by multi-channel TaqMan qPCR (McNew et al., 2018). Thermodynamic stability of each sequence was analyzed using Geneious 11.1 (Mathews et al., 2004) to ensure proper folding and robustness of the tracers.

2.2. DsDNA Tracer Quantification

Since there were eight different DNA sequences to test in each sample, we adopted the TaqMan probe method, which could detect multiple DNA sequences simultaneously and largely improved the testing efficiency compared with the SYBR Green method, which could only detect one DNA sequence per run (McNew et al., 2018). The Applied Biosystems QuantStudio 3 Real-Time PCR System we used could detect three different

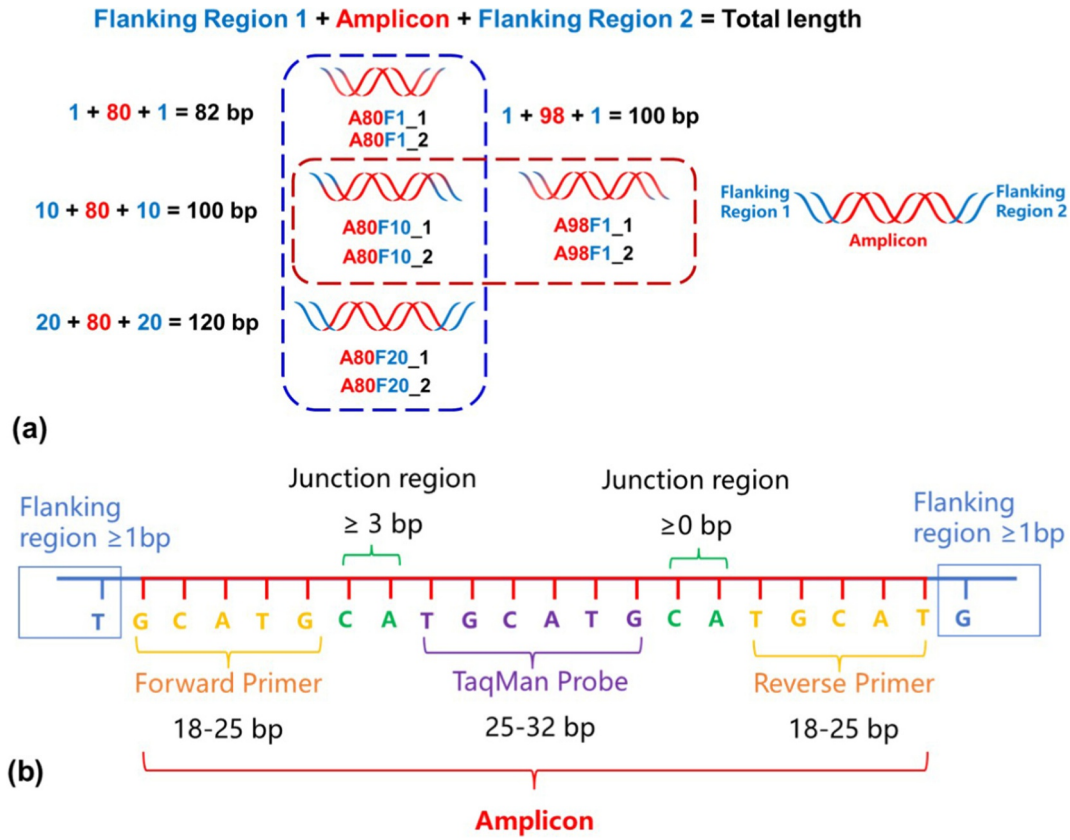

Figure 1. The three dsDNA tracer design parameters (i.e., amplicon length, flanking region length, and total DNA length) of our four pairs of dsDNA tracers (a) and the logic of their design (b).

DNA sequences simultaneously. The qPCR was performed using an Applied Biosystems QuantStudio 3 Real-Time PCR System under the following thermal cycling conditions: an initial denaturation at 95°C for 10 min, followed by 40 amplification cycles consisting of 95°C for 15 s and 60°C for 1 min. Each reaction consisted of 10 μL of the SsoAdvanced™ Universal probes Supermix, 6 μL of sample, and 4 μL of forward primer, reverse primer and TaqMan probe mixture. In the 4 μL mixture, the concentrations of the forward primer, reverse primer and TaqMan probe for each DNA tracer sequence were 2 μM, 2 μM, and 1 μM, respectively. Each sample together with triplicates of 7 standards (1E+09 copies/6 μL and its serial dilutions) and 1 negative control were included on each plate. Subsequently, the quantification cycle value of a 6 μL DNA sample was interpolated into the standard curve to estimate DNA copy counts, which would be converted to a concentration in copies/mL.

2.3. Sand and Water Samples

Two types of sand were chosen for the column breakthrough experiments to observe the breakthrough curves of the eight dsDNA tracers: (a) Ottawa sand (d_{50} = 0.240 mm, purchased from www.axner.com) and (b) a fine quartz sand (d_{50} = 0.110 mm, purchased from Gongyi Bangjie Water Purification Material Sales Co., Ltd., Zhengzhou, China). Ottawa sand has been successfully used in previous studies to differentiate the adsorption of dsDNA tracers with lengths varying from 90 to 200 bp (Zhang et al., 2021). The fine quartz sand was selected to check if the findings from the Ottawa sand can be reproduced in another type of sand. Both sands were washed with distilled water to remove fine particles (diameter <0.058 mm) and ions, then autoclaved, oven dried at 105°C and stored in a desiccator to keep dry. The differential and cumulative particle size distribution by volume of the Ottawa sand (Figure 2a) and the finer quartz sand (Figure 2b) were measured by a Mastersizer 2000 (Malvern, UK). For both the Ottawa sand (Figure 2c) and finer quartz sand (Figure 2d), the microscopic grain morphology was described by a scanning electron microscope (SEM). The specific surface area of the Ottawa sand (0.0358 m^2/g) and the fine quartz sand (0.1126 m^2/g) were characterized by Brunauer—Emmett—Teller (BET)—N_2 surface area measurement (Keiluweit et al., 2010). The mineral composition of the Ottawa sand was 99.8%

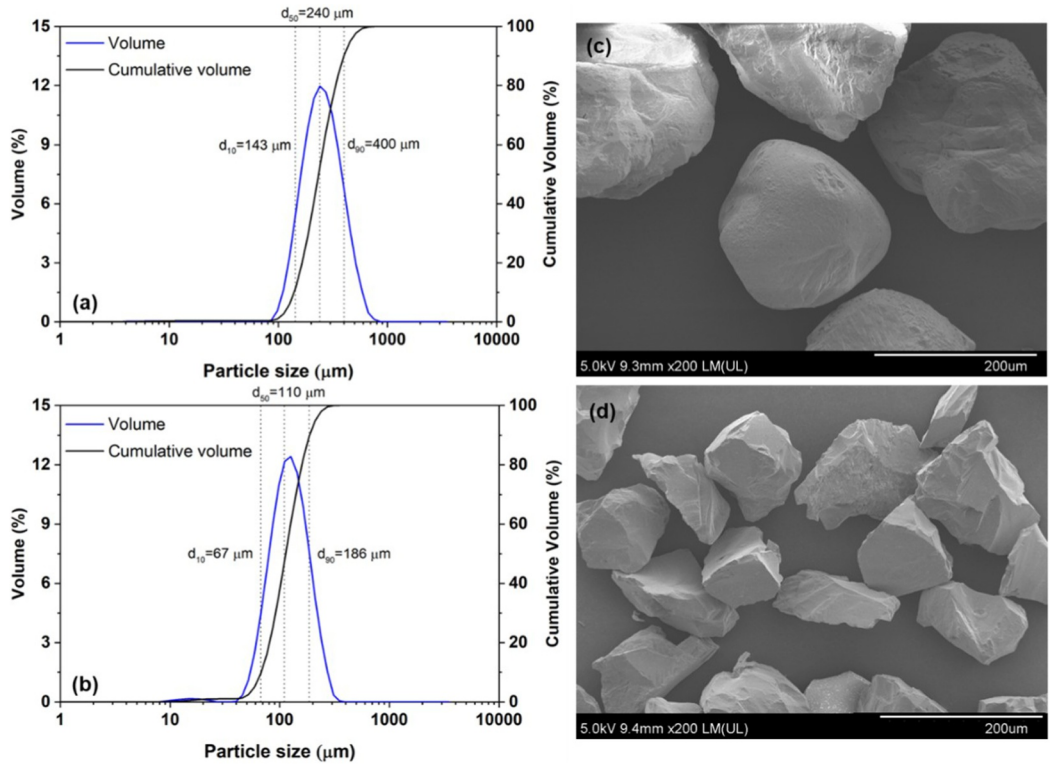

Figure 2. The differential and cumulative particle size distribution by volume of the Ottawa sand (a) and the finer quartz sand (b); and the microscopic morphology of the Ottawa sand grains (c) and the finer quartz sand grains (d).

quartz, 0.026% Fe_2O_3 and 0.051% Al_2O_3 (Axner, 2023). The X-ray diffraction analysis showed that the mineral composition of the finer quartz sand was 96.1% quartz and 3.9% mica.

To test if the absolute degradation rate would influence the relative order of degradation rate of dsDNA tracers of varying amplicon length, flanking region length or total length, two types of water with differing absolute degradation rates were used in the batch degradation experiments. One was farmland drainage water (2,600 colony forming unit (cfu)/mL) and the other was 2% biogas slurry (275,000 cfu/mL) (Table 2, heterotrophic plate count). This is because bacterial activity has been shown to be the primary water quality factor that controlling the absolute degradation rate of dsDNA tracers (Pang et al., 2022). The farmland drainage water was collected one day after a flood irrigation event from a drainage ditch (40°59′39″N, 107°20′54″E) at Hetao Irrigation District (HID) in Bayannur, Inner Mongolia Autonomous Region, China. The farmland drainage water can be regarded as the mixture of lateral discharge of shallow groundwater from nearby farmlands. Irrigation water used in this study was collected from a lined irrigation canal located adjacent to the drainage ditch. After collection, the farmland drainage water and irrigation water were stored at −20°C and thawed prior to the experiments, with a storage period of approximately two months. Biogas slurry is a wastewater byproduct generated during the anaerobic fermentation of animal manure, plant straw, or food waste, and diluted biogas slurry is commonly applied as a natural organic fertilizer for agricultural drip irrigation (Wang et al., 2024). In preliminary tests, free DNA degraded rapidly even in 5% biogas slurry, approaching the detection limit within 6 hr. Therefore, 2% biogas slurry was used to ensure measurable degradation during the experimental period. The raw biogas slurry was obtained from Beijing Miyun Haihua Baili Energy Technology Co., Ltd. (Wang, Wang, et al., 2022), stored at 4°C after collection for preservation of microbes, and used within approximately 1 month. It was diluted with irrigation water to 2% right before the degradation experiments. Typical water chemistry indicators of the drainage water and the 2% biogas slurry (Table 2) were measured with standard methods (Table S1 in Supporting Information S1).

Table 2
The Water Chemistry of the Drainage Water and the 2% Biogas Slurry

Parameter	Units	Drainage water	2% biogas slurry
pH		8.8	8.4
Heterotrophic plate count (35°C)	cfu[a]/mL	2,600	275,000
Conductivity	μS/cm	916	960
Potassium[b]	mg/L	5.45	–
Sodium[b]	mg/L	125.7	–
Calcium[b]	mg/L	55.96	–
Magnesium[b]	mg/L	44.37	–
Dissolved oxygen	mg/L	8.59	5.53
Total suspended particulate	mg/L	1,320	510
Total nitrogen	mg/L	1.4	3
Total phosphate	mg/L	2	27
Dissolved organic carbon	mg/L	30.91	44.52
Carbonaceous biochemical oxygen demand (20°C)	mg/L	8.58	61.7

[a]cfu: colony forming unit. [b]The concentration of Potassium, sodium, calcium, magnesium were only measured for the column experiment background solution, the drainage water.

2.4. Batch Degradation Experiments

Batch degradation experiments were conducted to measure the degradation rate of each of the 8 dsDNA tracers in two types of water with differing absolute degradation rates (farmland drainage water and 2% biogas slurry) under dark condition at a controlled temperature of 25.5 ± 0.03°C. For each degradation experiment, 100 mL of farmland drainage water or 2% biogas slurry was well mixed with 0.1 mL of each of the 8 dsDNA tracers, resulting in a 100.8 mL sample containing ~1E+10 copies/mL of each dsDNA tracers. A 0.8 mL initial sample was taken to measure the initial concentration (C_o, copies/mL), before it was divided into 10 tubes of 10 mL sample. Each tube was opened and used only once to take a sample right after thorough mixing to ensure that mixing and opening the tube would not interfere with the degradation process. Each sample was frozen at −20°C right after taken until the 8 dsDNA tracers were quantified with the method described in Section 2.2 DsDNA tracer quantification. Each degradation experiment lasted for 72 hr, and the samples were collected at 2, 4, 6, 8, 12, 24, 36, 48, 64, 72 hr. The first-order degradation was assumed following Pang et al. (2022), and the first-order degradation rate (λ, h^{-1}) of each dsDNA tracer in each of the two types of water was obtained by least-square fitting the first-order degradation equation (Equation S1 in Supporting Information S1) to the measured C/C_o versus t data (C is the concentration (copies/mL) at time t (hour)).

One-way ANOVA was used to examine, in each of the two types of water, whether there were significant differences in degradation rates between two dsDNA tracer groups with different amplicon lengths (80 bp vs. 98 bp), and whether there were significant differences in degradation rates among three dsDNA tracer groups with the same amplicon length (80 bp) but different flanking region lengths (1 bp vs. 10 bp vs. 20 bp). A significance threshold of $p < 0.05$ was adopted.

2.5. Column Breakthrough Experiments

The column breakthrough experiments were carried out using vertical 50 cm length and 1 cm inner diameter columns (Figure 3). Three of them were packed with Ottawa sand ($d_{50} = 0.240$ mm, Figures 2a and 2c) and the other three were packed with the finer quartz sand ($d_{50} = 0.110$ mm, Figures 2b and 2d) to study the dsDNA tracer properties in two types of sand. To ensure homogeneous sand columns, they were compacted by layers. All three Ottawa sand columns were packed to a bulk density (ρ_b) of 1.69 g/cm^3, resulting in a saturated water content (θ_s) of 0.362 cm^3/cm^3 and a pore volume (PV) of 15.23 cm^3. All three finer quartz sand columns were packed to a bulk density (ρ_b) of 1.33 g/cm^3, resulting in a saturated water content (θ_s) of 0.50 cm^3/cm^3 and a pore volume (PV) of 20.75 cm^3. The total surface area of the Ottawa sand and the fine quartz sand in the packed column were 2.53 and

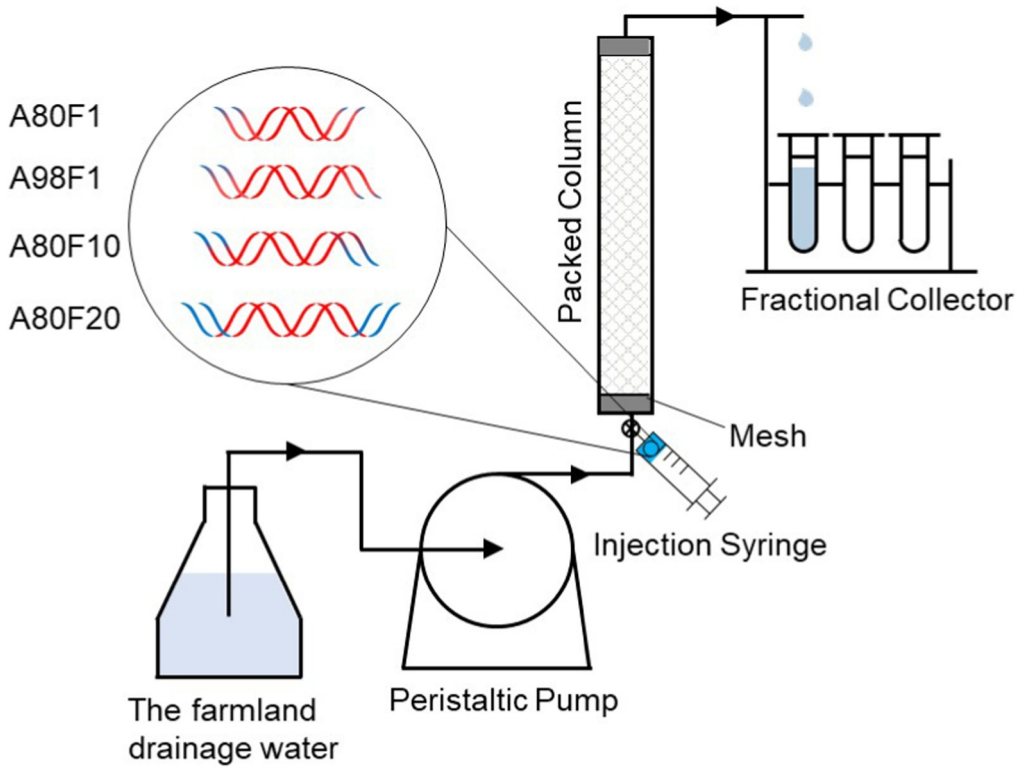

Figure 3. The column experiment setup. The column breakthrough experiment was repeated with three Ottawa sand columns and three finer quartz sand columns, a total of six experimental runs.

6.22 m^2, respectively, estimated by the weight of sand in the packed column and the measured specific surface area of the two types of sand.

Column breakthrough experiments were performed only using drainage water. Biogas slurry contains high concentrations of bacteria (275,000 cfu/mL) and other substances, which could strongly influence DNA adsorption and transport in porous media. Including biogas slurry in the column experiments would therefore obscure the intrinsic effects of DNA sequence length on adsorption behavior. Drainage water was thus selected as the background solution to investigate the influence of DNA tracer properties on transport processes.

We followed Aquilanti et al. (2013) and Zhang et al. (2021) for the free DNA tracer column breakthrough experiment setup, both of whom chose to inject free DNA tracer bottom-up through porous media, which was proved to be able to distinguish between dsDNA tracer of different length (Zhang et al., 2021). For each experimental run, one of the packed sand columns was flushed with >3 PV of farmland drainage water bottom-up using a peristaltic pump to achieve the same effluent pH as the influent pH (~8.8) and to prime the system to a saturated flow rate of about 0.6–0.7 cm/min. At t = 0, 1 mL tracer solution was injected at the bottom of the column instantaneously after taking an initial sample to determine the initial concentration (C_o) of each tracer. The tracer solution was obtained by mixing an equal-volume of the eight dsDNA tracer storage solutions (pH = 8.0) with pH = 8.0 Tris-HCl buffer containing a reference tracer KBr, to achieve a final concentration of ~2E + 14 copies/mL of each dsDNA tracer and 10 mmol/L of KBr. The drainage water was continuously flushed bottom-up with a constant flow rate until the end of the 1-hr experiment (equivalent to ~2.3 PV for Ottawa sand columns and ~1.8 PV for finer quartz sand columns), during which effluent water samples from the top of the column were collected with a fractional collector (Figure 3). The fractional collector was set to collect effluent continuously and switch to next tube every 2 minutes. In this way, all of the effluent from the column during the 1-hr experiment was collected and divided into 30 samples, each containing the effluent discharged in two minutes. The column experiments were conducted at room temperature (25.5°C). Each of the effluent samples were (a) quickly weighed to obtain the actual discharge, (b) a subsample was taken after thorough mixing and stored at −20°C until the measurement of the 8 dsDNA tracers using the method described in Section 2.2 DNA tracer

quantification, and (c) the rest was used for Br concentration measurements with an ion selective electrode (ISE, D10-35, Orion Dual Star, US) following Liu et al. (2023). After measuring the discharge and concentrations of Br and each of the 8 dsDNA tracers in each sample, the observed breakthrough curves can be obtained. Then, the observed recovery rates of Br and each of the 8 dsDNA tracers can be obtained by integrating the observed breakthrough curves, that is calculating the area under the observed breakthrough curves. And transport models can be inversely solved by fitting to the observed breakthrough curves.

2.6. DNA Tracer Fate and Transport Modeling

The governing equations of the two-site kinetic model are as follows:

$$\theta_s \frac{\partial C}{\partial t} + \rho_b \left(\frac{\partial S_1}{\partial t} + \frac{\partial S_2}{\partial t} \right) = \theta_s D^w \frac{\partial^2 C}{\partial x^2} - q \frac{\partial C}{\partial x} - \mu_w \theta_s C - \mu_s \rho_b (S_1 + S_2) \quad (1)$$

$$\rho_b \frac{\partial S_1}{\partial t} = \theta_s k_{a1} C - k_{d1} \rho_b S_1 - \mu_s \rho_b S_1 \quad (2)$$

$$\rho_b \frac{\partial S_2}{\partial t} = \theta_s k_{a2} C - k_{d2} \rho_b S_2 - \mu_s \rho_b S_2 \quad (3)$$

$$\theta_s D^w = D_L |q| + \theta_s D_w \tau_w \quad (4)$$

where C is the concentration of the dsDNA tracer in the aqueous phase (copies/mL), S is the concentration of the dsDNA tracer (copies/g) on sorption sites, given the saturated condition of our study, porosity θ_s is used to substitute the original water content θ in Equations 1–4, ρ_b is the dry bulk density (kg/m^3), D^w is the DNA dispersion coefficient tensor (cm^2/min), q is the Darcian fluid flux density (cm/min), D_L is the longitudinal dispersivity (cm), D_w is the DNA molecular diffusion coefficient in the aqueous phase (cm/min), τ_w ($=\theta_s^{7/3}/\theta_s^2 = \theta_s^{1/3}$) is a tortuosity factor (Millington & Quirk, 1961), μ_w and μ_s are the first-order degradation rates of the dsDNA tracer in the aqueous phase and on sorption sites (min^{-1}), respectively, k_a and k_d are the first-order attachment and detachment rate coefficients (min^{-1}), respectively, and subscripts 1 and 2 refer to the two kinetic sorption sites, respectively.

The one-site kinetic sorption model is a simplified form of the two-site kinetic sorption model in which all the items associated with subscript 2 are omitted. Following Eisfeld et al. (2022), besides the commonly used R^2 and Nash-Sutcliffe Efficiency (NSE, Equation S2 in Supporting Information S1), Akaike Information Criterion (AIC) was also used to select the best experiment validated model between the best fit one-site kinetic model and the best fit two-kinetic model. The model with a lower AIC performs better, because it balances the residual sum of squares (RSS) against model complexity, as represented by the number of adjustable parameters in the model (K):

$$\mathrm{AIC} = 2K + N \ln\left(\frac{\mathrm{RSS}}{N}\right) \quad (5)$$

where N is the number of data points to be fitted.

2.7. Inverse Modeling

To obtain the unknown parameters of the above physical-based equations, we used HYDRUS-1D to obtain the inverse solution. The domain setup and initial and boundary conditions of the HYDRUS-1D simulation are described in details in Text S4 in Supporting Information S1.

First, the variable flux head (q) was set to the measured discharge obtained by weighing each sample. Second, based on the measured flux and saturated water content (θ_s), the longitudinal dispersivity (D_L) of the conservative tracer Br and saturated hydraulic conductivity (K_s) were inversely solved by fitting them to the measured Br flux (please see Supporting Information S1 "S3. Reference Br tracer transport modeling" for details). Third, the degradation rate of the dsDNA tracer in the liquid phase (μ_w) was independently determined from batch degradation experiments and fixed in the model as the first-order degradation rate (λ, h^{-1}) obtained under dark conditions using farmland drainage water ($\mu_w = \lambda/60$, min^{-1}). Fourth, the degradation rate of the dsDNA tracer in

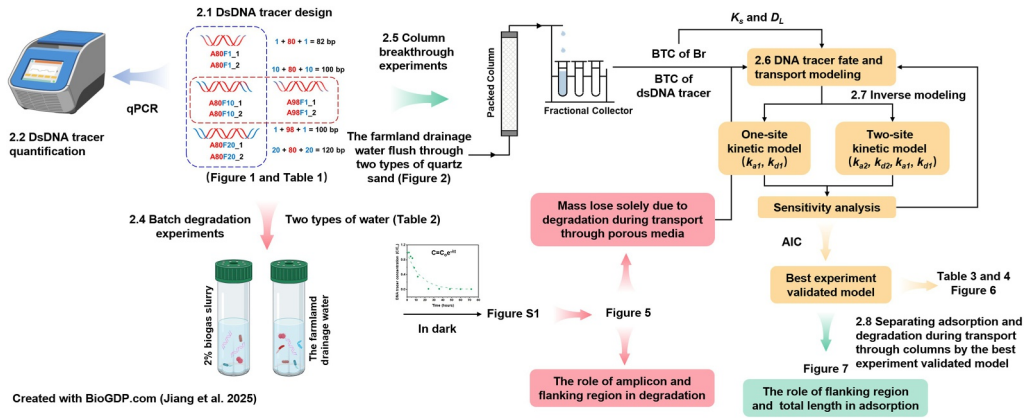

Figure 4. The relationships between the experiments and modeling, and the corresponding results of the experiments and modeling (Jiang et al., 2025).

the solid phase, that is, on sorption site(s) was set to be one order of magnitude lower than μ_w ($\mu_s = \mu_w/10$, min^{-1}) following Wang, Liu, et al. (2022) and Liu et al. (2023). Fifth, the molecular diffusion coefficient in the aqueous phase (D_w, cm^2/min) of each of the dsDNA tracers was obtained by determining the log-log linear relationship between the D_w and the total length of the dsDNA strand (N) found by Nkodo et al. (2001).

By independently constraining degradation parameters (μ_w and μ_s) and transport parameters (K_s and D_w) prior to inverse modeling, the number of free parameters during breakthrough curve fitting was substantially reduced, thereby improving parameter identifiability and minimizing equifinality.

Based on the above obtained saturated hydraulic conductivity (K_s), degradation rates (μ_w and μ_s) and diffusion coefficient (D_w), we used one-site and two-site kinetic sorption models to iteratively inversely solve for longitudinal dispersivity (D_L) and adsorption parameters of each dsDNA tracer by fitting to its breakthrough curve. As observed by Auset and Keller (2004) and validated by Pang et al. (2008), the longitudinal dispersivity of colloids is typically lower than that of conservative tracers. Therefore, D_L for each dsDNA tracer was iteratively reduced from the initial value (set equal to that of Br) until further reductions increased the Nash–Sutcliffe efficiency (NSE) by less than 1%. In each iteration, adsorption parameters (k_{a1} and k_{d1} for the one-site model; k_{a1}, k_{d1}, k_{a2}, and k_{d2} for the two-site model) were inversely estimated.

Similarly, adsorption parameters were sequentially updated based on sensitivity analysis, and iterations continued until further adjustments improved NSE by less than 1%. Through this stepwise and constrained inversion procedure, the number of simultaneously fitted parameters was limited to adsorption-related parameters only, ensuring a more robust and physically meaningful parameter estimation.

2.8. Quantitative Separation of Adsorption and Degradation During Column Transport

Degradation rates of the eight dsDNA tracers in farmland drainage water and 2% biogas slurry were determined in Section 2.4 (Figure 4). Breakthrough curves of the eight tracers through Ottawa sand and finer quartz sand in farmland drainage water were obtained in Section 2.5. One-site and two-site kinetic sorption models were subsequently inversely solved and evaluated, and the optimal model was selected as described in Sections 2.6 and 2.7.

Although both adsorption and degradation processes are explicitly represented in the transport model, the key advantage of the present approach lies in the independent experimental constraint of degradation parameters prior to model calibration. This enables a data-constrained partitioning of total mass loss during transport into degradation loss and adsorption loss, rather than relying on simultaneous parameter fitting, which often leads to non-unique solutions.

Specifically, adsorption ($M_{\text{adsorption}}$, %) was quantified by integrating the sorbed concentrations over the entire column domain at the end of the 1-hr experiment, normalized by the total injected mass. For the one-site model, adsorption was calculated from S_1, whereas for the two-site model it was calculated from (S_1+S_2). The

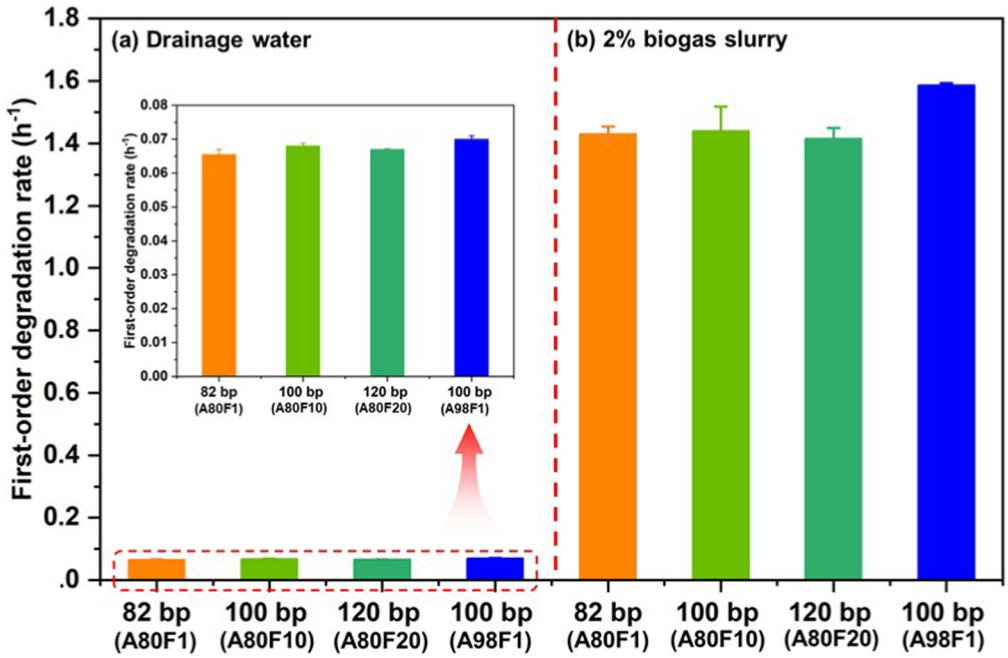

Figure 5. The mean and standard deviation of the first-order degradation rate (λ, h^{-1}) of the four pairs of dsDNA tracers in (a) farmland drainage water and (b) the 2% biogas slurry in the dark.

degradation loss during transport was quantified as the sum of degradation in pore water and degradation on sand surfaces. The degradation in pore water was represented by $\mu_w\theta_s C$ in Equation 1, and the cumulative degradation loss in water ($M_{\text{degraded in water}}$, %) was obtained by integrating $\mu_w\theta_s C$ over the entire column domain and experiment duration, normalized by the total injected mass.

Similarly, degradation of adsorbed dsDNA was represented by $\mu_s\rho_b S_1$ for the one-site model and $\mu_s\rho_b(S_1+S_2)$ for the two-site model. The cumulative degradation loss on sand surfaces ($M_{\text{degraded on sand}}$, %) was obtained by integrating these terms over space and time. Because degradation rates were independently determined and fixed, the remaining model-calibrated adsorption parameters exclusively describe adsorption and detachment processes. This allows for a physically interpretable and quantitatively robust separation of degradation and adsorption contributions to overall tracer attenuation during transport.

Importantly, this separation enables a more mechanistic interpretation of how the dsDNA tracer design parameters (i.e., amplicon length, flanking region length, and total length) individually control degradation and adsorption processes during subsurface transport. Without such decoupling, these effects would remain confounded within the integrated breakthrough response.

3. Results and Discussion

3.1. Degradation of dsDNA Tracer in Batch Experiments

The first-order degradation rate constants (Figure 5) were obtained by least-squares fitting of modeled degradation curves to the observed data (Figure S1 in Supporting Information S1). As expected, dsDNA tracers degraded substantially faster in the 2% biogas slurry (1.481 ± 0.076 hr^{-1}, Figure 5b) than in the farmland drainage water (0.068 ± 0.002 hr^{-1}, Figure 5a). This difference can be attributed to the higher bacterial concentration in the 2% biogas slurry (275,000 cfu/mL) compared with the drainage water (2,600 cfu/mL) (Table 2), which likely resulted in greater production of nucleases capable of degrading dsDNA (Torti et al., 2015).

Across both media, tracers containing an 80 bp amplicon exhibited consistently lower degradation rates than those containing a 98 bp amplicon. In drainage water, degradation rates were 0.067 ± 0.001 hr^{-1} for 80 bp amplicons and 0.070 ± 0.001 hr^{-1} for 98 bp amplicons ($p = 0.024$). Similarly, in 2% biogas slurry the degradation rates were 1.428 ± 0.018 hr^{-1} and 1.580 ± 0.006 hr^{-1} for the 80 bp and 98 bp amplicons, respectively ($p = 6.41 \times 10^{-4}$).

These results indicate that degradation rate is primarily controlled by the length of the amplicon rather than by the length of the flanking regions. Although absolute degradation rates differed between the two media, the relative order of tracer degradation remained consistent with amplicon length. This observation is consistent with previous findings (Mikutis et al., 2019), but here can be attributed specifically to amplicon length due to our dsDNA tracer design to disentangle previously confounded effects of amplicon length and total DNA length.

In contrast, tracers with identical amplicon lengths (80 bp) but different flanking region lengths (1, 10, and 20 bp on each side) showed no significant differences in degradation rates in either drainage water (0.066 hr^{-1} for A80F1, 0.067 hr^{-1} for A80F10, and 0.067 hr^{-1} for A80F20; $p = 0.110$) or 2% biogas slurry (1.431 hr^{-1}, 1.440 hr^{-1}, and 1.415 hr^{-1}, respectively; $p = 0.899$). These results demonstrate that extending flanking regions alone does not significantly enhance resistance to degradation.

This finding differs from that of Pang et al. (2022), who reported improved stability for tracers with longer flanking regions. In their study, longer flanking regions formed a terminal folded twin-stem-loop structure that substantially reduced the free energy of the dsDNA tracer (−92.9 vs. −62.4 kcal/mol), thereby increasing thermodynamic stability. In contrast, thermodynamic analysis of our tracers showed that sequences with identical amplicon length but different flanking region lengths had similar free energies (−16.43 ± 3.85 kcal/mol; $p = 0.575$). This indicates that our dsDNA tracers did not have stable secondary structures which could significantly lower the free energy.

These results address the research question regarding degradation protection: whether shortening the amplicon or extending flanking regions is more practical in protecting dsDNA tracers from degradation. Our findings suggest that controlling amplicon length is the dominant factor. Recent guidelines for synthetic DNA tracer design recommend avoiding stable secondary structures such as hairpins or folded twin-stem-loops to maintain high specificity and reliable detectability (Guo et al., 2025). Designing extended flanking regions that intentionally form secondary structures to improve stability could therefore compromise tracer specificity and qPCR detection. Consequently, adjusting the amplicon length represents a more practical and robust strategy for controlling the degradation behavior of synthetic DNA tracers.

3.2. Breakthrough of dsDNA Tracer Through Sand Columns

We obtained the breakthrough curves of Br and the 8 dsDNA tracers through the Ottawa sand (Figure 6a) and the finer quartz sand (Figure 6b) by taking the average of three experimental runs C/C_o measured at the same time (presented as pore volume). And the recovery rate of each of the dsDNA tracers (Table 3) was obtained by the total injection mass normalized integration of the breakthrough curves (C/C_o, Figures 6a and 6b). In Ottawa sand and the fine quartz sand, Br peaked at 1.16 PV (30 min) and 1.12 PV (38 min), with the recovery rates of 98.1% and 98.3% (Table 3), respectively (Figures 6a and 6b). The recovery rates of dsDNA tracers in the effluent were 49.2%–52.6% through the Ottawa sand columns and 23.1%–26.9% through the fine quartz sand columns. In the Ottawa sand column, dsDNA tracers peaked at 1.16 PV (30 min) with peak concentration (C_{max}/C_o) ranging from 0.13 to 0.167. In the fine quartz sand column, the peak occurred later at 1.18 PV (48 min) and had a lower peak concentration of 0.100–0.122 (Table 3 and Figure 6). The recovery rate of dsDNA tracer decreased with increase of total length through the Ottawa quartz sand column: 52.3% for the 82 bp DNA tracers, 50.9% for the 100 bp DNA tracers and 49.5% for the 120 bp DNA tracers. Similarly, the recovery rate of dsDNA tracer decreased with increase of total length through the finer quartz sand column: 26.1% for the 82 bp DNA tracers, 24.8% for the 100 bp DNA tracers and 24.0% for the 120 bp DNA tracers.

3.3. DsDNA Microscale Characterization and Adsorption Mechanisms

The persistence length of double stranded DNA is about 150 bp (50 nm; Smith et al., 1996), which means that double stranded DNA shorter than 150 bp is nearly rigid and hardly bend without outer forces. Our 82–120 bp dsDNA tracers are shorter than the persistence length of DNA, which means that they were essentially 2 nm diameter and 28–41 nm length (0.34 nm/bp) nano-rods (Smith et al., 1996). Thus, the retention of our dsDNA tracer did not follow the rules of flexible polymer flowing through porous media, that is, mechanical entrapment, hydrodynamic entrapment and adsorption (Sugar et al., 2023). According to McDowell-Boyer et al. (1986), when the ratio of porous media grain size (d_m) to the colloid particle size (d_p) is larger than 1,000, the retention of colloid particle would be dominated by physical-chemical filtration, while cake filtration and straining would be negligible. The colloid particle size of our dsDNA tracer could be roughly estimated as $d_p = 34.5$ nm (average of

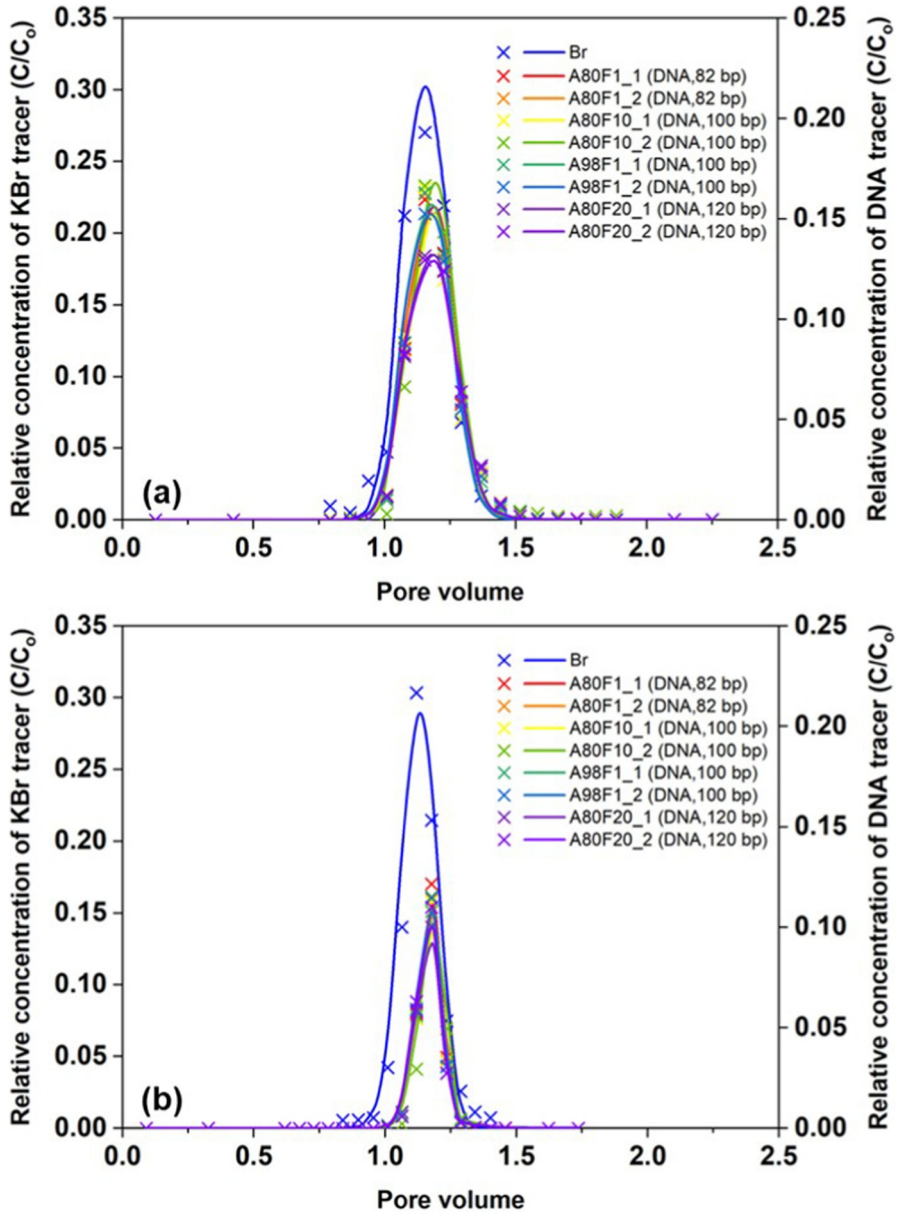

Figure 6. Observed and simulated, relative concentration of the reference Br tracer and the eight sequences of dsDNA tracers from (a) the triplicated Ottawa sand column experiments and (b) the triplicated finer quartz sand column experiments. The crosses represent the average of the triplicated experiments while the lines represent the model simulation. To maintain figure clarity, error bars were not added to the plot. The corresponding standard deviations for all triplicate measurements are tabulated in the archived data set (https://doi.org/10.5281/zenodo.17627923).

28 and 41 nm). The d_m of Ottawa sand and the fine quartz sand were 0.240 and 0.110 mm, respectively. Then the d_m/d_p were 6,857 and 3,143 for the Ottawa sand and the fine quartz sand, respectively, significantly larger than 1,000. This means that the filtration of the rod-shaped dsDNA would be dominated by the physical-chemical filtration, that is collide with the sand grains by sedimentation, interception or Brownian motion (McDowell-Boyer et al., 1986) and then, whether the dsDNA collide with the sand grains would attach to the sand grain would be determined by the adsorption mechanisms.

The isoelectric point (pI) of DNA is around 5 (Liu et al., 2023; Yu et al., 2013), which means that under our experimental condition (pH ~ 8.8), the dsDNA tracers were negatively charged. According to Emami et al. (2014) and Zhang et al. (2023), at our experimental pH (~8.8), the surface of quartz carries negative charge. Hence, our

Table 3
Peak Time (T_p), Peak Value (C_{max}/C_o), Recovery Rate ($M_{recovered}$), Adsorption ($M_{adsorption}$), Degradation Loss in Pore Water ($M_{degraded\ in\ water}$) and Degradation Loss on Sand Surface ($M_{degraded\ on\ sand}$) of dsDNA Tracers in the Ottawa Sand and the Finer Quartz Sand

Sample	Tracer name	T_p [a] (min)	(C_{max}/C_o) [a]	$M_{recoverd}$ [a] (%)	$M_{adsorption}$ [b] (%)	$M_{degraded\ in\ water}$ [b] (%)	$M_{degraded\ on\ sand\ surface}$ [b] (%)
Ottawa sand	Br	30	0.270 ± 0.044	98.1 ± 1.42	1.9		
	A80F1_1	30	0.160 ± 0.029	52.6 ± 3.41	48.51	0.88	0.42
	A80F1_2	30	0.162 ± 0.029	51.9 ± 3.66	47.40	0.86	0.41
	A80F10_1	30	0.165 ± 0.030	49.5 ± 1.65	53.39	0.87	0.48
	A80F10_2	30	0.167 ± 0.036	51.5 ± 0.39	48.36	0.93	0.45
	A98F1_1	30	0.163 ± 0.034	51.8 ± 2.40	46.99	0.95	0.43
	A98F1_2	30	0.153 ± 0.034	50.8 ± 2.83	47.76	0.96	0.46
	A80F20_1	30	0.135 ± 0.002	49.2 ± 0.86	51.23	0.85	0.46
	A80F20_2	30	0.130 ± 0.003	49.8 ± 1.09	54.40	0.86	0.49
The finer quartz sand	Br	38	0.303 ± 0.004	98.3 ± 0.24	1.7		
	A80F1_1	40	0.122 ± 0.037	26.9 ± 3.10	76.47	1.05	0.49
	A80F1_2	40	0.114 ± 0.032	25.3 ± 3.80	77.56	1.04	0.50
	A80F10_1	40	0.113 ± 0.037	25.3 ± 4.22	79.04	1.04	0.53
	A80F10_2	40	0.115 ± 0.034	23.9 ± 4.53	77.77	1.10	0.54
	A98F1_1	40	0.111 ± 0.038	24.4 ± 4.73	78.06	1.09	0.54
	A98F1_2	40	0.115 ± 0.029	25.6 ± 4.59	76.98	1.15	0.55
	A80F20_1	40	0.100 ± 0.042	23.1 ± 6.34	79.88	1.01	0.53
	A80F20_2	40	0.110 ± 0.042	24.8 ± 6.45	78.41	1.05	0.52

[a]Observed by triplicated column experiments. [b]Simulated with the best experiment validated model after model calibration and validation with experimental breakthrough curves.

dsDNA should not adsorb to quartz due to electrostatic repulsion. The mineral composition of Ottawa sand was 99.8% quartz, 0.026% Fe_2O_3 and 0.051% Al_2O_3 (Axner, 2023). Note, our experimental pH (~8.8) was even above the isoelectric point (pI) of the Fe_2O_3 (pI = 6.7 ± 1.6) and Al_2O_3 (pI = 8.3 ± 1.3) (Kosmulski, 2021). This means that even Fe_2O_3 and Al_2O_3 carried negative charge at our experimental pH. Then, how could the negatively charged dsDNA adsorb to the sand grains?

The answer was hidden in the farmland drainage water used for the column experiments, which contained 5.45 mg/L K^+, 125.7 mg/L Na^+, 55.96 mg/L Ca^{2+}, 44.37 mg/L Mg^{2+}, and 2 mg/L PO_4^{3-} (Table 2). The cations in the farmland drainage water could screen the negative charge and reduce the repulsion between the negatively charged DNA due to the phosphate backbone and the negatively charged quartz surface due to Si-O^- (Kushalkar et al., 2020). And the Ca^{2+} and Mg^{2+} could further form cation bridges between the negatively charged DNA and the negatively charged quartz. The X-ray diffraction analysis showed that the mineral composition of the finer quartz sand was 96.1% quartz and 3.9% mica. Thus, besides the adsorption mechanisms of the dsDNA to quartz, the dsDNA in the finer quartz sand could be adsorbed to the negatively charged mica (pI = 1.7 (Kosmulski, 2012)) as well.

3.4. Experiment Validated Modeling of dsDNA Tracer Transport Through Sand Columns

In both Ottawa sand and the finer quartz sand columns, the two-site kinetic sorption model performed better than the one-site kinetic sorption model, exhibiting lower AIC values alongside higher R^2 and NSE values. The two-site kinetic sorption model captured the breakthrough curves of the eight dsDNA tracers well in both Ottawa sand (R^2 = 0.96–0.99 and NSE = 0.96–0.99, AIC = −177.19–204.15, Figures 6a and 6b and Table 4) and the finer quartz sand (R^2 = 0.95–0.99 and NSE = 0.95–0.99, AIC = −190.51–220.09, Figures 6a and 6b and Table 4). The one-site kinetic sorption model satisfactorily captured the breakthrough curves of the eight dsDNA tracers well in the Ottawa sand column (R^2 = 0.92–0.98, NSE = 0.92–0.98, AIC = −171.08–190.46, Table 4), but could not perform satisfactorily in the finer quartz sand (R^2 = 0.82–0.98, NSE = 0.82–0.98, AIC = −170.82–217.64, Table 4). The better performance of the two-site kinetic sorption model showed that adding two parameters, k_{a2}

Table 4
Water Flow and dsDNA Tracer Transport Parameters

Porous media	Model	Tracer	K_s (cm/min)[a]	D_L (cm)[a]	D_w (cm^2/min)[b]	k_{a2} (min^{-1})[c]	k_{d2} (min^{-1})[c]	k_{a1} (min^{-1})[c]	k_{d1} (min^{-1})[c]	μ_w (min^{-1})[d]	μ_s (min^{-1})[d]	R^2	NSE	AIC
Ottawa sand		Br	0.62	0.153	1.03E−03	–	–	–	–	–	–	0.99	0.99	
	Two-site kinetic model	A80F1_1	0.62	0.138	1.26E−05	0.022	3.00E−04	0.068	3.98	1.08E−03	1.08E−04	0.98	0.98	−191.53
		A80F1_2	0.62	0.138	1.26E−05	0.022	3.00E−04	0.067	3.95	1.09E−03	1.09E−04	0.98	0.98	−189.26
		A80F10_1	0.62	0.138	1.13E−05	0.025	3.00E−04	0.055	2.93	1.12E−03	1.12E−04	0.96	0.96	−177.19
		A80F10_2	0.62	0.138	1.13E−05	0.022	3.00E−04	0.07	2.95	1.15E−03	1.15E−04	0.97	0.97	−177.97
		A98F1_1	0.62	0.138	1.13E−05	0.021	3.00E−04	0.055	2.98	1.15E−03	1.15E−04	0.98	0.98	−186.46
		A98F1_2	0.62	0.138	1.13E−05	0.022	3.00E−04	0.05	2.96	1.19E−03	1.19E−04	0.99	0.98	−190.12
		A80F20_1	0.62	0.138	1.01E−05	0.025	3.00E−04	0.045	1.6	1.11E−03	1.11E−04	0.99	0.99	−202.57
		A80F20_2	0.62	0.138	1.01E−05	0.026	3.00E−04	0.045	1.55	1.11E−03	1.11E−04	0.99	0.99	−204.15
	One-site kinetic model	A80F1_1	0.62	0.107	1.26E−05	–	–	0.024	7.35E−03	1.08E−03	1.08E−04	0.97	0.97	−184.68
		A80F1_2	0.62	0.107	1.26E−05	–	–	0.023	5.63E−03	1.09E−03	1.09E−04	0.97	0.97	−183.74
		A80F10_1	0.62	0.107	1.13E−05	–	–	0.025	4.83E−03	1.12E−03	1.12E−04	0.98	0.98	−190.46
		A80F10_2	0.62	0.107	1.13E−05	–	–	0.023	3.70E−03	1.15E−03	1.15E−04	0.95	0.94	−169.82
		A98F1_1	0.62	0.107	1.13E−05	–	–	0.026	1.01E−02	1.15E−03	1.15E−04	0.96	0.96	−176.63
		A98F1_2	0.62	0.107	1.13E−05	–	–	0.028	1.17E−02	1.19E−03	1.19E−04	0.96	0.95	−177.21
		A80F20_1	0.62	0.107	1.01E−05	–	–	0.031	1.44E−02	1.11E−03	1.11E−04	0.93	0.92	−171.08
		A80F20_2	0.62	0.107	1.01E−05	–	–	0.032	1.53E−02	1.11E−03	1.11E−04	0.92	0.92	−169.08
The finer quartz sand		Br	0.67	0.096	1.03E−03	–	–	–	–	–	–	0.97	0.96	
	Two-site kinetic model	A80F1_1	0.67	0.01	1.26E−05	0.042	3.00E−04	0.14	10.86	1.08E−03	1.08E−04	0.98	0.98	−207.42
		A80F1_2	0.67	0.01	1.26E−05	0.043	3.00E−04	0.139	10.85	1.09E−03	1.09E−04	0.98	0.98	−212.01
		A80F10_1	0.67	0.01	1.13E−05	0.045	3.00E−04	0.142	10.54	1.12E−03	1.12E−04	0.98	0.98	−206.96
		A80F10_2	0.67	0.01	1.13E−05	0.043	3.00E−04	0.261	10.55	1.15E−03	1.15E−04	0.95	0.95	−190.51
		A98F1_1	0.67	0.01	1.13E−05	0.044	3.00E−04	0.126	10.52	1.15E−03	1.15E−04	0.98	0.98	−215.34
		A98F1_2	0.67	0.01	1.13E−05	0.042	3.00E−04	0.118	10.53	1.19E−03	1.19E−04	0.98	0.98	−212.32
		A80F20_1	0.67	0.01	1.01E−05	0.047	3.00E−04	0.102	10.23	1.11E−03	1.11E−04	0.99	0.99	−220.09
		A80F20_2	0.67	0.01	1.01E−05	0.044	3.00E−04	0.093	10.24	1.11E−03	1.11E−04	0.98	0.98	−212.77
	One-site kinetic model	A80F1_1	0.67	0.002	1.26E−05	–	–	0.045	2.28E−03	1.08E−03	1.08E−04	0.96	0.96	−197.84
		A80F1_2	0.67	0.002	1.26E−05	–	–	0.045	2.99E−03	1.09E−03	1.09E−04	0.96	0.96	−198.48
		A80F10_1	0.67	0.002	1.13E−05	–	–	0.047	2.88E−03	1.12E−03	1.12E−04	0.96	0.96	−201.68
		A80F10_2	0.67	0.002	1.13E−05	–	–	0.049	5.12E−03	1.15E−03	1.15E−04	0.82	0.82	−170.82
		A98F1_1	0.67	0.002	1.13E−05	–	–	0.047	1.93E−03	1.15E−03	1.15E−04	0.97	0.97	−207.45
		A98F1_2	0.67	0.002	1.13E−05	–	–	0.045	1.77E−03	1.19E−03	1.19E−04	0.97	0.97	−207.72
		A80F20_1	0.67	0.002	1.01E−05	–	–	0.05	1.38E−03	1.11E−03	1.11E−04	0.98	0.98	−217.64
		A80F20_2	0.67	0.002	1.01E−05	–	–	0.047	1.07E−03	1.11E−03	1.11E−04	0.98	0.98	−214.86

Note. K_s is the saturated hydraulic conductivity, D_L is the longitudinal dispersivity, D_w is the diffusion coefficient, k_a and k_d are the attachment and detachment rate coefficients, respectively, and subscripts 1 and 2 refer to the two kinetic sorption sites, respectively. [a]Parameters were inversely solved by fitting to measured reference Br tracer breakthrough curve. [b]Prescribed parameter. [c]Parameters were inversely solved by fitting to measured dsDNA tracer breakthrough curve. [d]Parameters were derived from the batch degradation experiment in farmland drainage water in the dark.

and k_{d2}, could better capture the breakthrough curves of the dsDNA tracers. Sensitivity analysis of this best two-site kinetic sorption model (Figures S3–S5 in Supporting Information S1) showed that further adjusting any of the key parameters would not significantly improve the model performance, and in most cases would deteriorate the model performance, that is decrease the *NSE*. Sensitivity analysis of the best one-site kinetic sorption model shown in Table 4 (Figures S6–S8 in Supporting Information S1) also showed that further adjusting any of the key parameters would not effectively improve the model performance. Therefore, the two-site kinetic sorption model

shown in Table 4 was chosen as the best experiment validated model for further analysis and discussion. This is consistent with the findings of Schijven and Simunek (2002) who showed that the two-site kinetic sorption model performed significantly better one-site kinetic sorption model at capturing breakthrough curves of virus through porous media. Minor discrepancies between observations and model simulations are expected due to experimental variability and measurement uncertainty.

The one-site and two-site kinetic sorption models shared the same water flow parameters (Table 4). The saturated hydraulic conductivity ($K_s = 0.62$ cm/min for the Ottawa sand and $K_s = 0.67$ cm/min for the finer quartz sand) and the longitudinal dispersivity of conservative tracer Br ($D_L = 0.153$ cm for the Ottawa sand and $D_L = 0.096$ cm for the finer quartz sand) were inversely solved by fitting the advection-dispersion equation (Equation S2 in Supporting Information S1) to the measured Br breakthrough curve ($R^2 = 0.99$ and NSE = 0.99 for the Ottawa sand and $R^2 = 0.97$ and NSE = 0.96 for the finer quartz sand, Figures 6a and 6b and Table 4). Note that the grain size of the finer quartz sand was relatively uniform ($d_{10} = 67$ μm, $d_{50} = 110$ μm, $d_{90} = 186$ μm, Figure 2b). Whereas, the Ottawa sand had some larger sand grains and some smaller ones ($d_{10} = 143$ μm, $d_{50} = 240$ μm, $d_{90} = 400$ μm, Figure 2a), and the smaller ones can fit in between the larger ones. And this allowed the Ottawa sand to be more densely packed than the finer quartz sand, resulting in a larger bulk density ρ_b, lower saturated water content θ_s and, consequently, lower K_s than the finer quartz sand.

The one-site and two-site kinetic sorption model also shared the same degradation and diffusion parameters (Table 4). The degradation rates in the pore water (μ_w, min^{-1}) of the same dsDNA tracer were the same in both Ottawa sand and the finer quartz sand, because the μ_w was the degradation in pore water and thus determined by the pore water chemistry. Thus, the μ_w of each dsDNA tracer was the measured degradation rate of that dsDNA tracer in the farmland drainage water (λ, h^{-1}) converted to the unit of min^{-1}. The degradation rates of the attached dsDNA tracers were set to be $\mu_s = \mu_w/10$ following Wang, Liu, et al. (2022) and Liu et al. (2023). Sensitivity analysis showed that the best fit model was insensitive to μ_s as long as it was less than μ_w in both Ottawa sand and the finer quartz sand, that is the NSE of the model changed less than ±0.01% when μ_s changed from $\mu_w/10$ to $\mu_w/100$ (blue bars in Figures S5a and S5b in Supporting Information S1) or changed from $\mu_w/10$ to μ_w (orange bars in Figures S5a and S5b in Supporting Information S1). The molecular diffusion coefficient in the aqueous phase (D_w) of the four pairs of the dsDNA tracers increased with their total length, while the dsDNA tracers with the same total length had the same D_w in both types of quartz sand.

The eight dsDNA tracers shared the same longitudinal dispersivity (D_L) in the same sand column and in the same model (Table 4). In the Ottawa sand column, the D_L of the dsDNA tracers was slightly lower than the D_L of Br ($D_L = 0.153$ cm), and the D_L of the dsDNA tracers was slight lower in the one-site kinetic sorption model ($D_L = 0.107$ cm) than in the two-site kinetic sorption model ($D_L = 0.138$ cm). Whereas, in the finer quartz sand column, the D_L of the dsDNA tracers was 10 times lower than the D_L of Br ($D_L = 0.096$ cm), and the D_L of the dsDNA tracers was 5 times lower in the one-site kinetic sorption model ($D_L = 0.002$ cm) than in the two-site kinetic sorption model ($D_L = 0.01$ cm).

Interesting discoveries can be obtained from the attachment rates (k_{a1}, k_{a2}) and the detachment rates (k_{d1}, k_{d2}) of the best experiment validated model, that is the two-site kinetic sorption model demonstrated in Table 4. First, it was found that the k_{d2} was negligible compared to the k_{a2} for both the Ottawa sand and the finer quartz sand, indicating that kinetic sorption site 2 was an irreversible sorption site, which could be produced by the nanoscale charge heterogeneity on the surface of sand grains (Shen et al., 2018). Second, k_{d1} was 10–100 times larger than k_{a1} for both the Ottawa sand and the finer quartz sand, indicating that kinetic sorption site 1 was a reversible sorption site, which could be produced by nanoscale roughness induced shallow primary minimum interactions (Bradford et al., 2017; Liang et al., 2020). Most interestingly, the detachment rate coefficients (k_{d1}, y, min^{-1}) decreased linearly with the increase in total length of dsDNA tracer (x, bp) in both the Ottawa sand ($y = -0.0631x + 9.200$, $R^2 = 0.994$) and the finer quartz sand ($y = -0.0163x + 12.176$, $R^2 = 0.995$) (Table 4 and Figure 7a). This relationship is further examined in Section 3.5, where adsorption and degradation during column transport are separated using the best-performing model validated against experimental data.

3.5. Separated Adsorption and Degradation During Transport Through Columns by the Best Experiment Validated Model

The adsorption of the dsDNA tracers ($M_{\text{adsorption}}$) in the finer quartz sand was about 1.5 times of that in the coarser Ottawa sand (Table 3). This can be well explained by the over 2 times larger total sand grain surface area of the

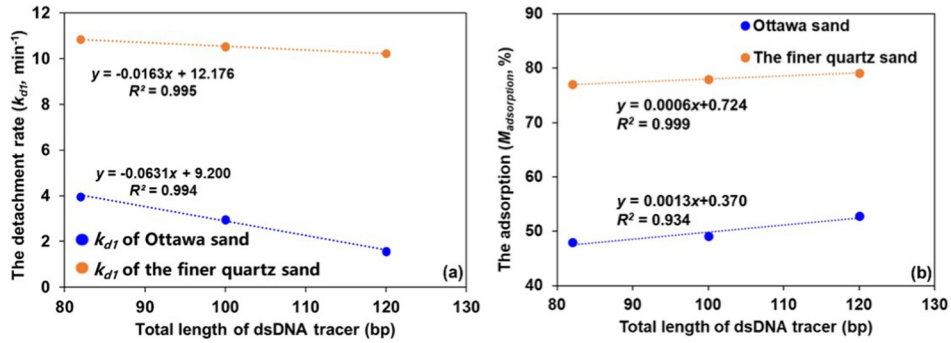

Figure 7. The detachment rate (k_{dl}) (a) and the adsorption ($M_{\text{adsorption}}$) (b) of the 8 dsDNA tracers of different total length in Ottawa sand and the finer quartz sand.

finer quartz sand column (6.22 m^2) than the Ottawa sand column (2.53 m^2). Most interestingly, the adsorption amount (y, %) increased linearly with the total length of dsDNA tracer (x, bp) in both Ottawa sand ($y = 0.0013x + 0.370$, $R^2 = 0.934$) and the finer quartz sand ($y = 0.0006x + 0.724$, $R^2 = 0.999$) (Figure 7b).

The linearly decreased detachment rate (Figure 7a) and the linearly increased adsorption (Figure 7b) together indicated that the number of binding sites is proportional to the total length of dsDNA tracer, and the probability of all of the binding sites to be detached from porous media decreases linearly with the increase in total length of dsDNA tracer. Our finding is consistent with Zhang et al. (2021) who also conducted column experiments and observed that longer polymers means more binding sites in quartz sand, but our results moved us one step further and determined a quantitative relationship between the total dsDNA tracer length and the detachment rate (k_{dl}; Figure 7a) and the linear relationship between the total dsDNA tracer length and the adsorption amount (%; Figure 7b). Thus, the adsorption of any dsDNA tracer can be controlled by its total length.

Surprisingly, although the degradation rate attached to sand was one order of magnitude lower than the degradation rate in pore water ($\mu_s = \mu_w/10$), the degradation loss of dsDNA attached to sand ($M_{\text{degraded on sand}}$) was about half of the degradation loss in pore water ($M_{\text{degraded in water}}$) in both Ottawa sand and the finer quartz sand (Table 3). This was because the adsorbed amount (the entire domain integration of (S_1+S_2)) was continuously increasing, while the dsDNA tracer amount in pore water (the entire domain integration of C) was continuously decreasing. The larger (S_1+S_2) in the finer quartz sand inevitably led to a larger $M_{\text{degraded on sand}}$ (integration of $\mu_s\rho_b(S_1+S_2)$) in the finer quartz sand. The $M_{\text{degraded in water}}$ of the finer quartz sand was also higher than that observed in the Ottawa sand (Table 3), because the dsDNA tracers passed through the coarser Ottawa sand (Figure 6a) faster than the finer quartz sand (Figure 6b), resulting in a lower C in the porous medium and lower integration of $\mu_w\theta_s C$.

4. Conclusions

This study disentangles the previously confounded effects of amplicon length, flanking region length, and total DNA length on the degradation and adsorption of synthetic dsDNA tracers during subsurface transport. By independently varying these three dsDNA tracer design parameters, we demonstrate that degradation is primarily controlled by amplicon length, whereas adsorption is governed by total DNA length. In contrast, flanking region length does not exert a measurable influence on either process when secondary structure formation is avoided. These findings resolve previously confounded relationships between DNA length and tracer behavior and provide a mechanistic basis for designing dsDNA tracers with predictable transport properties. Regarding degradation protection, our results demonstrate that the degradation rate of dsDNA tracers is primarily controlled by the length of the amplicon rather than the length of the flanking regions. Tracers with identical amplicon lengths but different flanking region lengths (A80F1, A80F10, and A80F20) showed similar degradation rates in both farmland drainage water and diluted biogas slurry. In contrast, the tracer with a longer amplicon (A98F1) degraded significantly faster than tracers containing an 80 bp amplicon under the same conditions. These findings indicate that shortening the amplicon is more practical than extending the flanking regions for improving resistance to degradation.

With respect to adsorption scaling, a clear and quantitative relationship between DNA length and adsorption behavior was established. Both experimental observations and model simulations consistently demonstrated that adsorption increased linearly with the total length of dsDNA tracers in the tested porous media. Specifically, the adsorption percentage exhibited a linear increase with total length in both Ottawa sand and finer quartz sand, whereas the detachment rate coefficient showed a linear decrease with increasing DNA length. Quantitatively, the adsorption fraction (y, %) scaled linearly with total dsDNA length (x, bp) in Ottawa sand ($y = 0.0013x + 0.370$, $R^2 = 0.934$) and finer quartz sand ($y = 0.0006x + 0.724$, $R^2 = 0.999$). While, the detachment rate coefficient (k_{d1}, y, min^{-1}) decreased linearly with DNA length in both Ottawa sand ($y = -0.0631x + 9.200$, $R^2 = 0.994$) and finer quartz sand ($y = -0.0163x + 12.176$, $R^2 = 0.995$). Collectively, these results indicate that total DNA length serves as a robust and predictive parameter for regulating adsorption and retention behavior during subsurface transport.

With respect to dsDNA tracer design parameters, our results show that when the total DNA length is fixed, the relative proportion of the amplicon length and flanking region length does not significantly affect adsorption behavior. Tracers A98F1 and A80F10, which had identical total lengths but different amplicon-to-flanking ratios, exhibited similar adsorption amounts and detachment rates in both types of sand media.

Based on these findings, clear design guidelines for dsDNA tracers emerge. Amplicon length should be selected to control degradation, with shorter amplicons reducing degradation rates. In contrast, total DNA length governs adsorption behavior, with shorter sequences exhibiting reduced adsorption during transport. Flanking regions primarily act as structural buffers and should be kept only as long as necessary to protect terminal nucleotides, without unnecessarily increasing total DNA length. Together, these results provide a mechanistic basis for designing dsDNA tracers with predictable transport behavior. It should be noted that this study examined tracer transport in only two types of sand media. Additional experiments in more complex porous materials, such as natural soils and aquifer sediments, will be necessary to further validate these findings before large-scale field applications of dsDNA tracers are recommended. More broadly, this framework highlights the importance of isolating the previously confounded effects of dsDNA tracer design parameters to enable predictive understanding of transport processes in complex subsurface systems.

Conflict of Interest

The authors declare no conflicts of interest relevant to this study.

Availability Statement

The data supporting the analysis and conclusions of this study is publicly available at https://doi.org/10.5281/zenodo.17627923 (Liu et al., 2026).

Acknowledgments

This work was supported by the Bayannaoer Research Institute Young Scientist Project [2024BYNECAU011]; the National Natural Science Foundation of China [52130902, 52579051]; the 2115 Talent Development Program of China Agricultural University [00109028]; the National Natural Science Foundation of China [51909264, 52279051, 52309068, 52579050], and a Heising–Simons Foundation [2014-59]. This work was also supported by the China Agricultural University Undergraduate Research Program [URP20201091002, X2021100190697]. The authors would like to thank Ruoyu Wang for purchasing Ottawa sand from the website www.axner.com and sending to China. Chaozi Wang, Geng Liu, Jiarong Liu, Zailin Huo, Guanhua Huang, Zengjie Hu, Yuhan Zhang, and Haoqi Guo are inventors of a Chinese patent (ZL202411782458.7) related to this work licensed to China Agricultural University on 09/23/2025.

References

Aquilanti, L., Clementi, F., Landolfo, S., Nanni, T., Palpacelli, S., & Tazioli, A. (2013). A DNA tracer used in column tests for hydrogeology applications. *Environmental Earth Sciences*, *70*(7), 3143–3154. https://doi.org/10.1007/s12665-013-2379-y

Aquilanti, L., Clementi, F., Nanni, T., Palpacelli, S., Tazioli, A., & Vivalda, P. M. (2016). DNA and fluorescein tracer tests to study the recharge, groundwater flowpath and hydraulic contact of aquifers in the Umbria-Marche limestone ridge (central Apennines, Italy). *Environmental Earth Sciences*, *75*(7), 626. https://doi.org/10.1007/s12665-016-5436-5

Auset, M., & Keller, A. A. (2004). Pore-scale processes that control dispersion of colloids in saturated porous media. *Water Resources Research*, *40*(3). https://doi.org/10.1029/2003WR002800

Axner. (2023). Laguna Clay Company - FL: Sand - Silica Sand F-65 Ottawa (sold per lb).

Bradford, S. A., Kim, H., Shen, C., Sasidharan, S., & Shang, J. (2017). Contributions of nanoscale roughness to anomalous colloid retention and stability behavior. *Langmuir*, *33*(38), 10094–10105. https://doi.org/10.1021/acs.langmuir.7b02445

Dahlke, H. E., Williamson, A. G., Georgakakos, C., Leung, S., Sharma, A. N., Lyon, S. W., & Walter, M. T. (2015). Using concurrent DNA tracer injections to infer glacial flow pathways. *Hydrological Processes*, *29*(25), 5257–5274. https://doi.org/10.1002/hyp.10679

Eisfeld, C., Schijven, J. F., van der Wolf, J. M., Medema, G., Kruisdijk, E., & van Breukelen, B. M. (2022). Removal of bacterial plant pathogens in columns filled with quartz and natural sediments under anoxic and oxygenated conditions. *Water Research*, *220*, 118724. https://doi.org/10.1016/j.watres.2022.118724

Emami, F. S., Puddu, V., Berry, R. J., Varshney, V., Patwardhan, S. V., Perry, C. C., & Heinz, H. (2014). Force field and a surface model database for silica to simulate interfacial properties in atomic resolution. *Chemistry of Materials*, *26*(8), 2647–2658. https://doi.org/10.1021/cm500365c

Foppen, J. W. (2023). Artificial DNA in hydrology. *WIREs Water*, *10*(6), e1681. https://doi.org/10.1002/wat2.1681

Guo, J., Wang, A., Liao, R., Yan, J., Li, X., Kang, Y., et al. (2025). An optimization generator of synthetic DNA fragments for the rational design of environmental tracers. *ACS Nano*, *19*(9), 9412–9421. https://doi.org/10.1021/acsnano.5c01980

Jiang, S., Li, H., Zhang, L., Mu, W., Zhang, Y., Chen, T., et al. (2025). Generic Diagramming Platform (GDP): A comprehensive database of high-quality biomedical graphics. *Nucleic Acids Research*, *53*(D1), D1670–D1676. https://doi.org/10.1093/nar/gkae973

Jiang, W., Liang, P., Wang, B., Fang, J., Lang, J., Tian, G., et al. (2015). Optimized DNA extraction and metagenomic sequencing of airborne microbial communities. *Nature Protocols*, *10*(5), 768–779. https://doi.org/10.1038/nprot.2015.046

Keiluweit, M., Nico, P. S., Johnson, M. G., & Kleber, M. (2010). Dynamic molecular structure of plant biomass-derived black carbon (Biochar). *Environmental Science & Technology*, *44*(4), 1247–1253. https://doi.org/10.1021/es9031419

Kosmulski, M. (2012). IEP as a parameter characterizing the pH-dependent surface charging of materials other than metal oxides. *Advances in Colloid and Interface Science*, *171–172*, 77–86. https://doi.org/10.1016/j.cis.2012.01.005

Kosmulski, M. (2021). The pH dependent surface charging and points of zero charge. IX. Update. *Advances in Colloid and Interface Science*, *296*, 102519. https://doi.org/10.1016/j.cis.2021.102519

Kushalkar, M. P., Liu, B. W., & Liu, J. W. (2020). Promoting DNA adsorption by acids and polyvalent cations: Beyond charge screening. *Langmuir*, *36*(38), 11183–11195. https://doi.org/10.1021/acs.langmuir.0c02122

Li, X., Duan, Z., Liao, R., Šimůnek, J., Han, Y., & Yang, D. (2025). Synthetic DNA fragments as high-resolution tracers for hydrological parameter inversion. *Geophysical Research Letters*, *52*(14), e2025GL116820. https://doi.org/10.1029/2025gl116820

Liang, Y., Zhou, J., Dong, Y., Klumpp, E., Šimůnek, J., & Bradford, S. A. (2020). Evidence for the critical role of nanoscale surface roughness on the retention and release of silver nanoparticles in porous media. *Environmental Pollution*, *258*, 113803. https://doi.org/10.1016/j.envpol.2019.113803

Liao, R., Yang, P., Wu, W., Luo, D., & Yang, D. (2018). A DNA tracer system for hydrological environment investigations. *Environmental Science & Technology*, *52*(4), 1695–1703. https://doi.org/10.1021/acs.est.7b02928

Liu, G., Guo, L., Wang, C., Liu, J., Hu, Z., Dahlke, H. E., et al. (2023). Revealing the infiltration process and retention mechanisms of surface applied free DNA tracer through soil under flood irrigation. *Science of the Total Environment*, *905*, 167378. https://doi.org/10.1016/j.scitotenv.2023.167378

Liu, G., Wang, C., & Huo, Z. (2026). Breakthrough curves and degradation curves [Dataset]. *Zenodo*. https://doi.org/10.5281/zenodo.17627923

Masaki, Y., Onishi, Y., & Seio, K. (2022). Quantification of synthetic errors during chemical synthesis of DNA and its suppression by non-canonical nucleosides. *Scientific Reports*, *12*(1), 12095. https://doi.org/10.1038/s41598-022-16222-2

Mathews, D. H., Disney, M. D., Childs, J. L., Schroeder, S. J., Zuker, M., & Turner, D. H. (2004). Incorporating chemical modification constraints into a dynamic programming algorithm for prediction of RNA secondary structure. *Proceedings of the National Academy of Sciences*, *101*(19), 7287–7292. https://doi.org/10.1073/pnas.0401799101

McDowell-Boyer, L. M., Hunt, J. R., & Sitar, N. (1986). Particle transport through porous media. *Water Resources Research*, *22*(13), 1901–1921. https://doi.org/10.1029/WR022i013p01901

McNew, C. P., Wang, C., Walter, M. T., & Dahlke, H. E. (2018). Fabrication, detection, and analysis of DNA-labeled PLGA particles for environmental transport studies. *Journal of Colloid and Interface Science*, *526*, 207–219. https://doi.org/10.1016/j.jcis.2018.04.059

Mikutis, G., Schmid, L., Stark, W. J., & Grass, R. N. (2019). Length-dependent DNA degradation kinetic model: Decay compensation in DNA tracer concentration measurements. *AIChE Journal*, *65*(1), 40–48. https://doi.org/10.1002/aic.16433

Millington, R. J., & Quirk, J. P. (1961). Permeability of porous solids. *Transactions of the Faraday Society*, *57*, 1200. https://doi.org/10.1039/tf9615701200

NCBI. (2023). National center for biotechnology information (NCBI) database.

Nkodo, A. E., Garnier, J. M., Tinland, B., Ren, H., Desruisseaux, C., McCormick, L. C., et al. (2001). Diffusion coefficient of DNA molecules during free solution electrophoresis. *Electrophoresis*, *22*(12), 2424–2432. https://doi.org/10.1002/1522-2683(200107)22:12<2424::AID-ELPS2424>3.0.CO;2-1

Pang, L., Abeysekera, G., Hanning, K., Premaratne, A., Robson, B., Abraham, P., et al. (2020). Water tracking in surface water, groundwater and soils using free and alginate-chitosan encapsulated synthetic DNA tracers. *Water Research*, *184*, 116192. https://doi.org/10.1016/j.watres.2020.116192

Pang, L., Heiligenthal, L., Premaratne, A., Hanning, K. R., Abraham, P., Sutton, R., et al. (2022). Degradation and adsorption of synthetic DNA water tracers in environmental matrices. *Science of the Total Environment*, *844*, 157146. https://doi.org/10.1016/j.scitotenv.2022.157146

Pang, L., McLeod, M., Aislabie, J., Šimůnek, J., Close, M., & Hector, R. (2008). Modeling transport of microbes in ten undisturbed soils under effluent irrigation. *Vadose Zone Journal*, *7*(1), 97–111. https://doi.org/10.2136/vzj2007.0108

Pang, L., Robson, B., Farkas, K., McGill, E., Varsani, A., Gillot, L., et al. (2017). Tracking effluent discharges in undisturbed stony soil and alluvial gravel aquifer using synthetic DNA tracers. *Science of the Total Environment*, *592*, 144–152. https://doi.org/10.1016/j.scitotenv.2017.03.072

Ptak, T., Piepenbrink, M., & Martac, E. (2004). Tracer tests for the investigation of heterogeneous porous media and stochastic modelling of flow and transport—A review of some recent developments. *Journal of Hydrology*, *294*(1–3), 122–163. https://doi.org/10.1016/j.jhydrol.2004.01.020

Romanowski, G., Lorenz, M. G., & Wackernagel, W. (1993). Use of polymerase chain reaction and electroporation of Escherichia coli to monitor the persistence of extracellular plasmid DNA introduced into natural soils. *Applied and Environmental Microbiology*, *59*(10), 3438–3446. https://doi.org/10.1128/aem.59.10.3438-3446.1993

Sabir, I. H., Haldorsen, S., Torgensen, J., Aleström, P., Gaut, S., Colleuille, H., et al. (2000). Synthetic DNA tracers: Examples of their application in water related studies. *Tracers and Modelling in Hydrogeology*, *262*, 159–165.

Sabir, I. H., Torgersen, J., Haldorsen, S., & Aleström, P. (1999). DNA tracers with information capacity and high detection sensitivity tested in groundwater studies. *Hydrogeology Journal*, *7*(3), 264–272. https://doi.org/10.1007/s100400050200

Schijven, J. F., & Simunek, J. (2002). Kinetic modeling of virus transport at the field scale. *Journal of Contaminant Hydrology*, *55*(1–2), 113–135. https://doi.org/10.1016/S0169-7722(01)00188-7

Shen, C., Bradford, S. A., Li, T., Li, B., & Huang, Y. (2018). Can nanoscale surface charge heterogeneity really explain colloid detachment from primary minima upon reduction of solution ionic strength? *Journal of Nanoparticle Research*, *20*(6), 165. https://doi.org/10.1007/s11051-018-4265-8

Smith, S. B., Cui, Y. J., & Bustamante, C. (1996). Overstretching B-DNA: The elastic response of individual double-stranded and single-stranded DNA molecules. *Science*, *271*(5250), 795–799. https://doi.org/10.1126/science.271.5250.795

Sugar, A., Serag, M., Buttner, U., Habuchi, S., & Hoteit, H. (2023). A single-molecule study on polymer fluid dynamics in porous media. *Lab on a Chip*, *23*(18), 4104–4116. https://doi.org/10.1039/d3lc00467h

Suzuki, T., Ohsumi, S., & Makino, K. (1994). Mechanistic studies on depurination and apurinic site chain breakage in oligodeoxyribonucleotides. *Nucleic Acids Research*, *22*(23), 4997–5003. https://doi.org/10.1093/nar/22.23.4997

Torti, A., Lever, M. A., & Jørgensen, B. B. (2015). Origin, dynamics, and implications of extracellular DNA pools in marine sediments. *Marine Genomics*, *24*, 185–196. https://doi.org/10.1016/j.margen.2015.08.007

Wang, C., Liu, G., McNew, C. P., Volkmann, T. H. M., Pangle, L., Troch, P. A., et al. (2022). Simulation of experimental synthetic DNA tracer transport through the vadose zone. *Water Research*, *223*, 119009. https://doi.org/10.1016/j.watres.2022.119009

Wang, H., Wang, H., Liang, X., Wang, J., Qiu, X., Wang, C., & Li, G. (2024). Infiltration simulation and system design of biogas slurry drip irrigation using HYDRUS model. *Computers and Electronics in Agriculture*, *218*, 108682. https://doi.org/10.1016/j.compag.2024.108682

Wang, H., Wang, J., Wang, C., Wang, S., Qiu, X., Sun, Y., & Li, G. (2022). Characterization of labyrinth emitter-clogging substances in biogas slurry drip irrigation systems. *Science of the Total Environment*, *820*, 153315. https://doi.org/10.1016/j.scitotenv.2022.153315

Yu, W. H., Li, N., Tong, D. S., Zhou, C. H., Lin, C. X., & Xu, C. Y. (2013). Adsorption of proteins and nucleic acids on clay minerals and their interactions: A review. *Applied Clay Science*, *80*(81), 443–452. https://doi.org/10.1016/j.clay.2013.06.003

Zhang, H. L., Xu, Z. J., Sun, W., Zhu, Y. G., Chen, D. X., & Zhang, C. Y. (2023). Hydroxylation structure of quartz surface and its molecular hydrophobicity. *Applied Surface Science*, *612*, 155884. https://doi.org/10.1016/j.apsusc.2022.155884

Zhang, Y., Hartung, M. B., Hawkins, A. J., Dekas, A. E., Li, K., & Horne, R. N. (2021). DNA tracer transport through porous media—The effect of DNA length and adsorption. *Water Resources Research*, *57*(2), 1–15. https://doi.org/10.1029/2020wr028382

Zhang, Y., & Huang, T. (2022). DNA-based tracers for the characterization of hydrogeological systems—Recent advances and new frontiers. *Water*, *14*(21), 3545. https://doi.org/10.3390/w14213545

References From the Supporting Information

Reading, L. P., Baumgartl, T., Bristow, K. L., & Lockington, D. A. (2012). Applying HYDRUS to flow in a sodic clay soil with solution composition–dependent hydraulic conductivity. *Vadose Zone Journal*, *11*(2), vzj2011.0137. https://doi.org/10.2136/vzj2011.0137

Saito, T., & Doi, H. (2021). Degradation modeling of water environmental DNA: Experiments on multiple DNA sources in pond and seawater. *Environmental DNA*, *3*(4), 850–860. https://doi.org/10.1002/edn3.192

Yaws, C. L. (2009). *Transport properties of chemicals and hydrocarbons*. C. L. Yaws (ed) (pp. 594–596). William Andrew Publishing. https://doi.org/10.1016/B978-0-8155-2039-9.50018-1